Self-Contained, Biomolecular Motor-Driven Protein Sorting and Concentrating in an Ultrasensitive Microfluidic Chip

ARTICLE *in* NANO LETTERS · MAY 2008

Impact Factor: 13.59 · DOI: 10.1021/nl072742x · Source: PubMed

4 AUTHORS, INCLUDING:

Chih-Ting Lin
National Taiwan University
70 PUBLICATIONS **399** CITATIONS
SEE PROFILE

Katsuo Kurabayashi
University of Michigan
138 PUBLICATIONS **1,687** CITATIONS
SEE PROFILE

NANO LETTERS

2008
Vol. 8, No. 4
1041-1046

Self-Contained, Biomolecular Motor-Driven Protein Sorting and Concentrating in an Ultrasensitive Microfluidic Chip

Chih-Ting Lin,[†] Ming-Tse Kao,[‡] Katsuo Kurabayashi,[*,§] and Edgar Meyhofer[*,‡,§]

Department of Mechanical Engineering, University of Michigan, Ann Arbor, Michigan 48109

Received October 23, 2007; Revised Manuscript Received February 7, 2008

ABSTRACT

We developed a molecular sorter that operates without external power or control by integrating the microtubule-based, biological motor kinesin into a microfluidic channel network to sort, transport, and concentrate molecules. In our devices, functionalized microtubules that capture analyte molecules are steered along kinesin-coated microchannel tracks toward a collector structure, concentrated, and trapped. Using fluorescent analyte molecules and nanoliter sample volumes, we demonstrated 14 fM sensitivity, even in the presence of high concentrations of other proteins.

On-chip high-throughput, ultrasensitive screening and biodetection for emerging diagnostic applications and innovative scientific discovery require micro- to nanofluidic systems for detecting analyte concentrations in the nano- to picomolar range. Low volume technology is essential to match the conditions governed by the size and molecular complexity of tissues and cells. It also promises the sensitivity, cost, and speed advantages associated with small scales. However, crucial challenges in such high-throughput analytic methods arise because (1) very small fluid volumes need to be shuttled through complex devices and (2) target molecules at low concentrations need to be recognized, sorted, and (pre)concentrated for reliable detection or synthesis. For example, friction against fluid transport increases dramatically at low Reynolds numbers, thus limiting sample delivery driven by conventional mechanical fluid powering components. Few approaches appear to be suitable to selectively detect, manipulate, and transport specific molecules in complex high-throughput devices, largely because the required local control is not feasible. Inspired by biological transport in cells, one novel concept to address these emerging biotechnology challenges proposes to integrate biomolecular motors into engineered on-chip structures (for a recent review, see ref 1). These systems are used to shuttle cargoes, sort and transport molecules, and power fluid motion in nano- and microfluidic systems. Several biomolecule-based specific transporters have been proposed by different research groups,[2–4] and first steps toward this technology have been realized (for example, see ref 5). However, significant progress is necessary before practical applications, like on-chip molecular sorters and concentrators, can be implemented. As a critical milestone toward realizing these applications, we set out to design and implement arrays of microfluidics-based, ultrasensitive device structures that are functionalized by biomolecular motors. We propose to use these devices to autonomously sort, transport, and concentrate protein target molecules without the use of external power or control.

Biomolecular motors, also referred to as motor proteins, are efficient, robust, and versatile nanoscale protein machines ubiquitous to all eukaryotic cells. They are responsible for vesicle transport, cell division, cellular motility, and muscle contraction.[6,7] Among the various motor proteins, we employ conventional kinesin (kinesin-1) for the proposed transport and actuation mechanisms in micro- and nanofluidic systems because it works reliably as a single molecule, cooperatively interacts in multimotor complexes, and can be readily genetically engineered and expressed in bacteria. Kinesin interacts and moves along microtubules in 8 nm steps by alternatively advancing its two motor domains coupled to the hydrolysis of adenosine triphosphate (ATP).[8,9] This chemomechanical transduction mechanism is intriguing from an application standpoint as it eliminates the need for external power sources. Other advantages of the kinesin−microtubule

* Corresponding Author. E-mail: katsuo@umich.edu or meyhofer@umich.edu
† Department of Electrical Engineering and Computer Science, University of Michigan.
‡ Department of Biomedical Engineering, University of Michigan.
§ Department of Mechanical Engineering, University of Michigan.

10.1021/nl072742x CCC: $40.75
Published on Web 03/05/2008

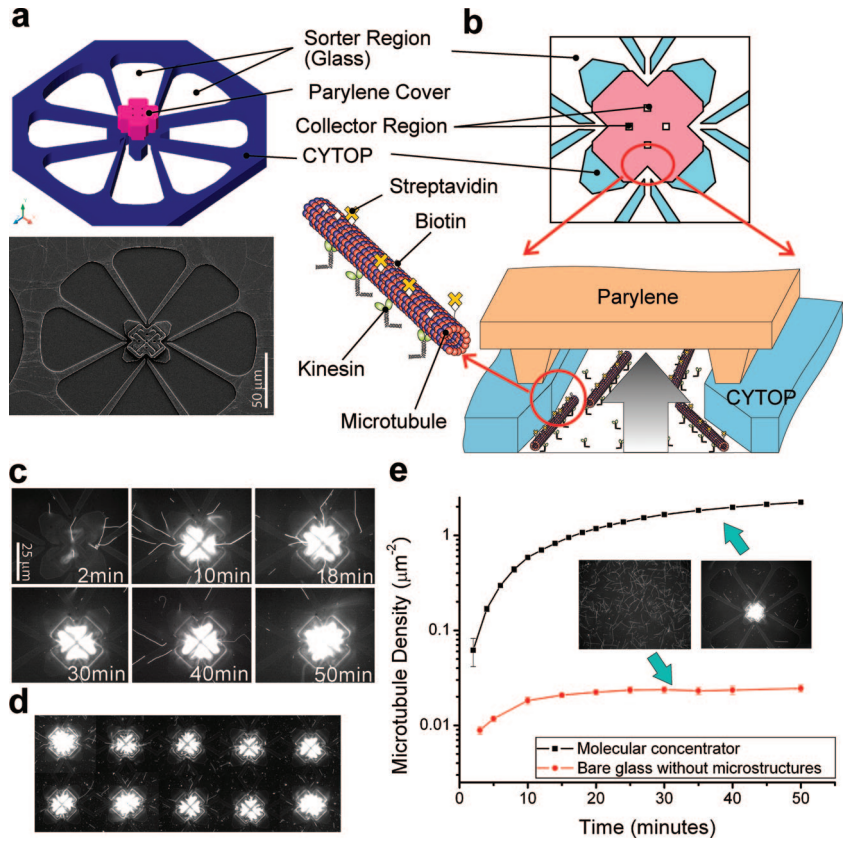

Figure 1. Design of biomolecular motor-based sorter and concentrator. (a,b) Design concept and structure of the microfluidic device. A schematic overview of a single sorting and concentrating structure (3D representation and SEM image) is shown in (a), and the detailed structure and functional concept for the collector structure are depicted in (b). Bioconjugated microtubules land in the sorter regions and are transported by kinesin toward the collector region. The total device area is 25600 μm^2, and the central collector region measures 372 μm^2. A parylene layer on the top of the collector serves as cover to prevent microtubule loss from the collector region. Highly selective motility in the sorter region is achieved by employing CYTOP as a structural material for all guiding structures throughout the device. (c) Representative time sequence demonstrating the rapid collection of microtubules in the device structure (see also Supporting Information movie 2, which, in addition, establishes device array uniformity). After 40 min of operation, the MT density in the collector part (d) is approximately 2 orders of magnitude higher than that on bare glass without microstructures. This microtubule concentrating effect is quantitatively demonstrated in (d) by comparing the microtubule density in our microfabricated device with a bare glass surface as a function of time.

system include the highly processive movement of kinesin along microtubules (MT)[10–12] and the relatively large size and robustness of microtubules as compared to other cytoskeletal tracks. Furthermore, the movement of microtubules can be rectified and steered with lithographically patterned channel tracks[13–16] and electric fields.[5,17,18] Selective cargos, including biomolecules and nanoparticles, can be conjugated to and transported with microtubules.[19–21]

Here we report the development of a new microfluidic device that contains a large array of kinesin and microtubule-based detectors, each independently capable of ATP-fueled autonomous molecular sorting, transport, and concentrating of target analytes. In our current design, the spacing between individual detectors was 250 μm, leading to a total of 1600 detectors and a typical fluid volume of 20–30 μL for a total array area of 1 cm^2. The basic design of a single detector is shown in Figure 1. These detectors function by incorporating microtubules in carefully designed, kinesin-coated microchannel tracks as molecular shuttles to transport cargo. The microtubules are functionalized to selectively bind protein cargo molecules from a dilute sample solution and are transported by surface-immobilized kinesin motors to a collector region that traps them.

Our device consists of a glass substrate, petal-shaped channels etched into a hydrofluorocarbon polymer (CYTOP) film, and the aforementioned micrometer-scale trap region with a parylene cap (Figure 1a,b). We named the petal-shaped channels and the trap region "sorter" and "collector," respectively. Kinesin motor molecules were preloaded into the microfluidic device and adsorbed to all exposed glass surfaces of the microchannels and traps. Previously, we discovered that CYTOP polymer surfaces, in contrast to glass, yield nonmotile surfaces for kinesin-driven microtubules,[16] presumably because of the very low adsorption of kinesin to the hydrophobic hydrofluorocarbon surface. Using this motility contrast between the hydrofluorocarbon and glass surfaces, we were able to selectively confine the binding and gliding of microtubules to the glass microchannels in our device. When microtubules are introduced to the device in a buffer solution, they diffuse to the kinesin-coated sorter surfaces, bind to kinesins, and move in the presence of ATP. Upon reaching a hydrofluorocarbon polymer channel walls,

the microtubules were redirected and guided toward the collector region by fully mechanical processes. The geometry of the device was optimized to facilitate the binding, guiding and trapping of microtubules. First, the large cross-section and petal shape of the microchannels of each detector were optimized to provide a sizable microtubule landing zone and to prevent the loss of microtubules at sharp corners (see ref 16). Second, the distinctive arrow-shaped patterns in the trap region effectively permit only one-way entry of microtubules, thereby keeping the collected microtubules from escaping through the entrances. Through this process, analyte molecules specifically bound to functionalized microtubule shuttles can be collected and concentrated in the collector region.

To quantitatively characterize the microtubule transport and concentration performance in our device structures, we fluorescently labeled microtubules with tetramethylrhodamine (TMR), loaded them in an ATP-containing physiological solution into the kinesin-functionalized device, and traced their motions via fluorescence microscopy. As predicted, microtubules rapidly accumulated in the collector (Figure 1c,d and Supporting Information movie 1). The fluorescence intensity in the collector region increased rapidly in the first 10–15 min; after about 45 min, it appeared to markedly saturate. Utilizing fluorescent microscopy, we were also able to count the number of microtubules approaching the collector entrance and found that 830 ± 25 (mean $\pm$ standard deviation, $N = 3$) microtubules were fully trapped within the collector after 50 min of operation. At the same time, there were only 29 ± 1.4 (mean $\pm$ standard deviation) microtubules left in the much larger sorter regions, further highlighting the concentration capability of the collector structure. Furthermore, we compared the microtubule density on bare glass surfaces without microstructures to the collector region (Figure 1e). The results show that our devices yield about 100-fold higher microtubule density in the collector region, indicating a concentrating capability of the devices with a gain of 100. Previous work has shown that microtubule attachment and detachment rates determine an equilibrium surface density on bare glass.[16] For the detector structures used in this work, the large petal-shaped sorter regions quickly reduced the local microtubule concentration in solution. Combined with the rapid transport of microtubules to the collector, this led to a pronounced depletion of microtubules in the sorter (see Figure 1e). This in turn caused the slowed increase of microtubules in the collector after 20 min of operation. As a whole, these observations strongly indicate that our detector structures very efficiently direct a large number of microtubule shuttles to the collector.

To demonstrate high-sensitivity protein detection with our devices, we used biotinylated microtubules and TMR-labeled streptavidin (TMR-STV). The use of the biotin−streptavidin linkage is a common approach for loading cargoes onto microtubules and has been employed in previous studies to transport CdSe quantum dots,[19] microspheres,[22] and DNA molecules.[23] Also, streptavidin has recently been used successfully to immobilize commercially available, biotinylated antibodies onto biotinylated microtubule shuttles.[21] As such, the biotin−streptavidin system provides a model broadly applicable to immunobased detection. In our assay, biotinylated microtubules were first loaded into the device with a physiological buffer solution containing ADP (Figure 2a). The presence of ADP inhibits microtubule motility on the kinesin-coated surface of the sorter region. Subsequently, our model analyte (TMR-STV) was loaded at varying concentrations while allowing the analyte molecules to selectively bind to the functionalized microtubules. After an incubation period of 1 min, an ATP-containing solution was loaded into the device to initiate microtubule motility. At this point, the analyte molecules were sorted from the general protein mixture and selectively concentrated in the collector region (Figure 2b). Our measurements of the spatially averaged fluorescence intensity of TMR-STV molecules in the collector demonstrate that the recorded signals vary linearly with the TMR-STV concentration in the observed range from 14 nM down to 14 fM (Figure 2c). Control experiments without microtubules verify that the major fractions of the observed signals are the result of the microtubule-based transport to the collector. Also, the background signal is well below the signals recorded even for femtomolar analyte concentrations. To quantitatively examine aspects of the protein detection mechanism and modulate the sensitivity of our detector, we sequentially loaded multiple (flow cell) volumes into the chip while keeping the microtubules in each individual detector immobilized to the kinesin-coated surface in the presence of ADP. The observed parallel shift of the sensitivity curves (Figure 2c) illustrates that the number of collected analyte molecules sharply increases with repeated analyte sample loading steps and resulting increasing sample volumes. This suggests that much higher signal-to-noise ratios and sensitivity (Figure 2d) can be achieved, presumably because analyte molecules are integrated to vacant binding sites available on each biotinylated microtubule for the capture and transport of TMR-STV analyte molecules. Utilizing this enhanced methodology, we could achieve 2 orders of magnitude higher detection sensitivity than typical existing immunoassays employing enzyme-linked immunosorbent assay, ELISA.[24]

Finally, we verified the cargo specificity of our technique by including multiple nonanalyte protein species (besides TMR-STV analyte) in sample solution. First, we added fluorescein-labeled bovine serum albumin (FITC-BSA) at 15 nM to the TMR-STV solution and applied the same assay protocol as above. The different spectral excitation and emission characteristics of TMR and FITC fluorophores allowed us to differentiate the on-chip distribution of these protein species. The data clearly indicate that the STV molecules were carried to the collector region by the biotinylated microtubules with no measurable effect on the spatial distribution of the BSA molecules (Figure 3a−d). Within a 95% confidence interval, no significant variations in location and time were found for the fluorescence intensity from FITC-BSA at the varying TMR-STV concentration. Additional measurements using a physiological (blood plasma) concentration, approximately 85 μM (Figure 3e), show that the characteristic detection responses (measured

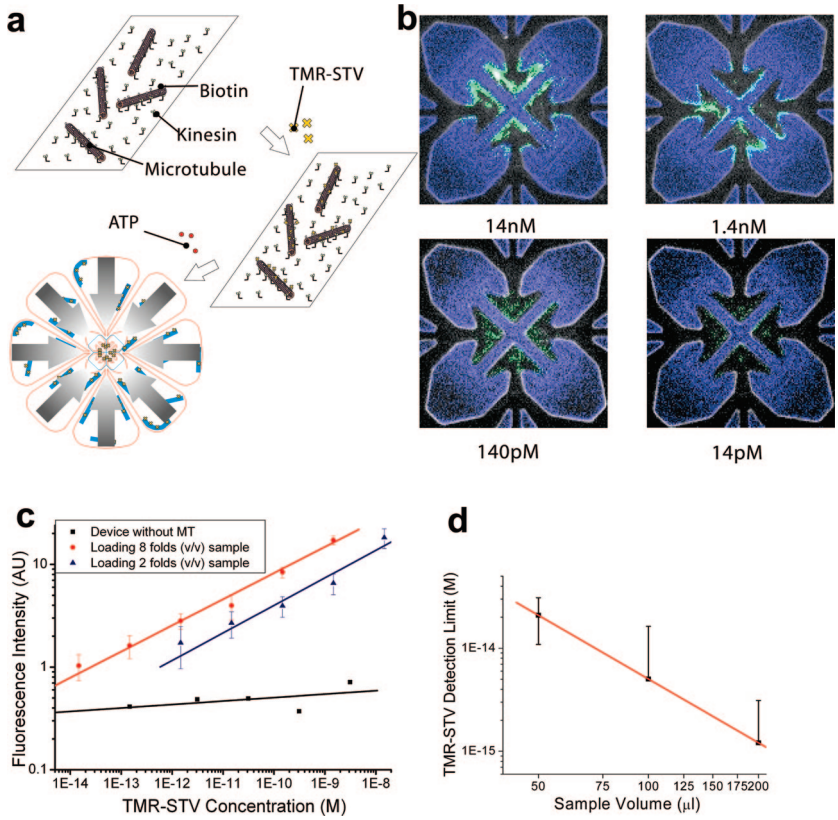

Figure 2. Molecular sorting and sensitivity of biomolecular motor-based microfluidic device. Tetramethylrohodamine-labeled strepavidin (TMR-STV) was used as a model system to experimentally characterize the molecular detectors. The experimental protocol is summarized in (a). Microtubules land and bind to surface-bound kinesins in the absence of ATP fuel. Subsequently, analyte solution is loaded into the device, and finally ATP is loaded to start the sorting and concentration process. Optical images of the collector region (b) show visibly different accumulations of TMR-STV as a function of analyte concentration in the range from 14 pM to 14 nM. The microfabricated structure is presented in blue, and the fluorescence from TMR-STV is marked in green. (c) Sensitivity of the devices in arbitrary units (AU) in the range from 10 fM to 10 nM ($N = 8$ for each concentration, error bars indicate standard deviations). The red and blue curves indicate experimental results observed by loading a total of 8 and 2 flow cell sample volumes, respectively, into the device. Control experiments in the absence of biotinylated microtubules (black curve) show that the detected signals are specific. By loading multiple samples volumes into our microfluidic chip, it is possible to fine-tune the sensitivity of the device. We characterized the detection limit of the device (d) from the intercept of the sample sensitivity curve (as shown in c) and the control measurements of the absence of biotinylated microtubules. The errors of the detection limit at different sample concentration (as shown in d) were estimated from the statistical uncertainties of the intercept of the sample sensitivity curves. The data in (d) indicate that the sensitivity of our biomolecular motor-driven detector is in the lower femtomolar range. As each microfluidic chip contains about 3200 individual devices, averaging of the signals from the individual detector will virtually eliminate the possibility of false-positive detections and dramatically reduce the detection limit of the device, probably well into the attomolar range.

fluorescence intensity vs analyte concentration) are independent of the presence of nonanalyte BSA proteins. In addition, glucose oxidase and catalase, which are usually included in physiological buffers of fluorescent motility assays as part of an antibleaching system, did not effect the sorting and transport capabilities of our devices. These observations strongly support the view that our kinesin- and microtubule-based molecular sorters are highly specific and selective, and are generally not influenced by background proteins.

Our biomolecular motor-based assay is a novel alternative to other existing, high-sensitivity methods utilizing nanoparticles,[25] nanowires,[26] microcantilevers,[27] quartz crystal microbalances[28] or surface plasmon resonance.[29] Our detection strategy, which is based on seamlessly integrating kinesin-driven, bioconjugated microtubule shuttles in microfluidic chips, is uniquely capable of molecular cargo sorting, transporting, and collecting in protein assays without any laborious, biochemical surface modifications, fluidic manipulations, electrical wiring, or signal processing that are required for many conventional methods.

In summary, we demonstrated the use of biotinylated, microtubule-based molecular shuttles for practical on-chip sorting, transporting, and concentrating of fluorescently labeled streptavidin in a microfluidic device. The assays reported here demonstrate that our unique microfluidic tracks are capable of efficiently trapping nearly 10^3 molecular shuttles in a $20 \times 20\ \mu m^2$ collector region in a 50 min period of autonomous, self-powered operation. The analyte concentration process in each microfluidic sorter and collector allows detection of analytes at concentrations as low as 14 fM with excellent cargo selectivity and regular flow-through sample loading. Moreover, the small operational volume of each sorter and collector structure (~10 nL for the current design) is ideally suited for high-throughput, high-content array detectors and redundant testing to eliminate false-positive tests on a single chip. In fact, during the work

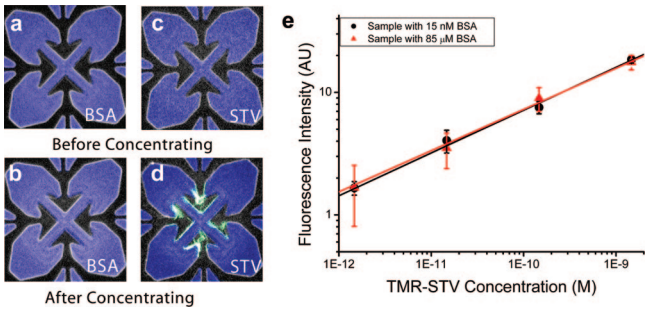

Figure 3. Device selectivity. We experimentally demonstrated the analyte selectivity of our devices by mixing TMR-STV with an FITC-labeled background protein, BSA, by using the standard protocol and identical devices. TMR-labeled STV signals were measured by green wavelength excitation, and FITC-labeled BSA signals were recorded by blue wavelength excitation. (a−d) Fluorescence micrographs of an experiment to detect 1.4 nM TMR-STV in the presence of 15 nM FITC-BSA. The collector microstructure is presented in light-blue color, and TMR-STV is shown in light-reen color. (e) Device sensitivity is not affected by background protein at different concentrations of BSA ranging from 15 nM FITC-BSA ($N = 12$, black) to 85 μM BSA ($N = 12$, red).

reported here, we observed that virtually every single sorter and collector structure behaved identically, indicating that both the devices and assays are very robust. We also note that the volume of microfluidic devices with single detection structures can be readily reduced to the pL range by matching the length scales to those of eukarytic cells (10–100 μm). Combining such device structures with the femtomolar sensitivity of our sorting and concentrating devices should, for example, make it possible to detect molecules from individual cells present in relatively small copy numbers. Furthermore, we suggest that self-assembled and autonomously operating, hybrid biomolecular and microfluidic systems hold significant potential for future developments of complex, high-throughput, point-of-care, biodiagnostic techniques

Methods. Device Fabrication. To fabricate the collector device, we first prepared a cover glass substrate using piranha clean and HF (1:20 diluted) surface treatment. This was followed by spin-coating of the clean glass substrate with a CYTOP (Asahi Glass Co.) film of about 1 μm thickness at 3000 rpm and curing of the CYTOP film at 180 °C for 30 min in an oven. CYTOP channels were patterned by lithography and plasma etching using SF_6 gas at a pressure of 20 mTorr, an RF etching power of 120 W, and a gas flow rate of 20 sccm (standard cubic centimeters per minute).[16] After stripping the photoresist remaining from the previous lithography process, new photoresist was spun onto the substrate as a sacrificial layer and patterned such that the required collector structures form when a parylene layer was subsequently deposited. Adhesion between parylene and CYTOP was increased by an oxygen descum (80 W, 250 mT, and 90 s). Parylene was deposited and patterned by plasma etching using O_2 gas at a 100 mTorr pressure, 150 W etching power, and a gas flow rate of 100 sccm. Finally, all photoresist was stripped using PRS2000 and the devices were carefully rinsed in DI water to free the CYTOP and parylene sorter and collector structures from sacrificial photoresist layers.

Protein Preparation. For our experiments, we used a bacterially expressed kinesin motor, NKHK560cys. This motor consists of the head and neck domain of *Neurospara crassa* kinesin (amino acids 1–433), the stalk of *Homo sapiens* kinesin (residues 430−560), and a reactive cysteine at the C-terminal end. The NKHK560cys gene was ligated into the pT77 plasmid and expressed in *Eschirichia coli* BL21 cells using TPM medium with 50 μM ampicillin at 37 °C. Expression was induced by adding 0.1 mM IPTG at a cell density corresponding to an OD of 0.6–0.8 and continued overnight at 22 °C. Cells were centrifuged and resuspended in lysis buffer containing protease inhibitors, DNase, and lysozyme followed by sonification. The supernatant of this extract was loaded on SPFF ion exchanger (Amersham Biosciences), and kinesin was eluted by a step gradient protocol. Tubulin and TMR-labeled tubulin were obtained by standard procedures. Briefly, tubulin was purified from cow brain by three cycles of microtubule polymerization and depolymerization followed by phosphocellulose ion exchange chromatography to eliminate microtubule associate proteins. Tubulin was labeled with TMR (Molecular Probes) by reacting polymerized microtubules with a 20-fold excess of dye at room temperature for 30 min. Competent, labeled tubulin was purified from this mixture by repeated depolymerization and polymerization.

Experimental Protocol. Microtubules were polymerized by incubating 2.4 mg/mL tubulin, 1 mM GTP, and 4 mM $MgCl_2$ in BRB80 buffer at 37 °C for 20 min and subsequently stabilized by adding 10 μM taxol. Microtubule biotinylation was achieved by incubating microtubules with 100 μM biotin-XX succinimidyl ester (B-1606, Invitrogen) for 30 min at room temperature. Unreacted biotin was quenched with 1 mM K-glutamate for 10 min and removed by repeated (4 times) microtubule pelleting in an airfuge (Beckman Instruments, 164000*g*, 5 min) and resuspension in BRB80 buffer with taxol. Flow chambers were constructed from microscope slides and microfabricated cover glasses containing the collector devices separated by ∼100 μm thickness double side tapes (Scotch 3M). To reduce the fluorescence background, some devices (when indicated) were bleached by exposing them for 20 min to the arc-lamp excitation of the fluorescence microscope. Devices were pretreated by flushing 100 μL of a 40 mg/mL aqueous solution of Pluronic (Pluronic F108 Prill, BASF) through the microfluidic chip. Protein loading was identical to that for standard kinesin gliding assays: Chambers were loaded with kinesin (0.4 mg/mL Pluronic and 2.1 μM kinesin in BRB80 buffer) and incubated for 5 min. During this incubation, a reference picture was taken and the reference intensity was measured from the collector region. Then, biotinylated microtubules (9.6 μg/mL tubulin) in a BRB80 buffer containing 10 μM taxol, 1 mM ATP, and an oxygen scavenger system) were loaded into the chip and incubated for 3 min. The chamber was loaded with various TMR-streptavidin concentrations (1 mM ADP, 2 mM $MgCl_2$, 10 mM glucose, 100 μg/mL glucose oxidase, 80 μg/mL catalase,

10 mM DTT, and 0.4 mg/mL Pluronic) and incubated for 1 min. Then, a microtubule motility solution (1 mM ATP, 2 mM $MgCl_2$, 10 mM glucose, 100 μg/mL glucose oxidase, 80 μg/mL catalase, 10 mM DTT, and 0.4 mg/mL Pluronic) was loaded into the chip and incubated for 5 min. Samples were observed with an inverted fluorescence microscope (Zeiss Axiovert 200, 40×/1.3 NA Plan Neofluar objective), and images were recorded with a digital CCD camera (Orca ER, Hamamatsu, Japan). The average fluorescence intensity difference was determined by subtracting reference intensity from the final experimental picture.

Acknowledgment. We acknowledge financial support from DARPA (E.M., K.K.), NSF (E.M., K.K.), and NIH (EM).

Supporting Information Available: Movie 1: Video sequences of the self-contained microtubule concentrating process in a microfluidic device. The movie was captured using a 100× oil-immersion objective (Plan-Neofluar, Zeiss) showing the central collector region of an active sorter device at high resolution. Microtubules were labeled with TMR and loaded into devices following the kinesin coating step. The cross-shaped portion in the image represents the collector region and the light gray regions are the CYTOP microstructures. The movie shows that microtubules in the peripheral sorter region of the device are guided to move into the collector region. Most microtubules are rapidly trapped in the collector, only very few of them escape. Movie 2: Comparison of multiple sorter devices of a large array. The movie was recorded with a lower magnification oil objective (40× Plan-Neofluar, Zeiss) to show entire devices with their sorter and collector regions. Microtubules were labeled with TMR and loaded into devices after the kinesin coating step. The movie sequence was recorded following a short transport and sorting period after the activation of the microfluidic chips. To show multiple neighboring sorters in an array, we rapidly translated the microfludic chip with the microscope stage. The sequence demonstrates that all individual sorting devices in the array transported microtubules and function in an identical manner. This material is available free of charge via the Internet at http://pubs.acs.org.

References

(1) van den Heuvel, M. G.; Dekker, C. *Science* **2007**, *317* (5836), 333–336.
(2) Jia, L. L.; Moorjani, S. G.; Jackson, T. N.; Hancock, W. O. *Biomed. Microdev.* **2004**, *6* (1), 67–74.
(3) Yokokawa, R.; Takeuchi, S.; Kon, T.; Nishiura, M.; Sutoh, K.; Fujita, H. *Nano Lett.* **2004**, *4* (11), 2265–2270.
(4) Hess, H.; Bachand, G. D.; Vogel, V. *Chem.—-Eur. J.* **2004**, *10* (9), 2110–2116.
(5) van den Heuvel, M. G. L.; De Graaff, M. P.; Dekker, C. *Science* **2006**, *312* (5775), 910–914.
(6) Hirokawa, N.; Noda, Y.; Okada, Y. *Curr. Opin. Cell Biol.* **1998**, *10* (1), 60–73.
(7) Alberts, B., *Molecular Biology of the Cell*, 4th ed.; Garland Science: New York, 2002; pp xxxiv, 1548.
(8) Hua, W.; Young, E. C.; Fleming, M. L.; Gelles, J. *Nature* **1997**, *388* (6640), 390–393.
(9) Coy, D. L.; Wagenbach, M.; Howard, J. *J. Biol. Chem.* **1999**, *274* (6), 3667–3671.
(10) Vale, R. D.; Schnapp, B. J.; Mitchison, T.; Steuer, E.; Reese, T. S.; Sheetz, M. P. *Cell* **1985**, *43* (3), 623–632.
(11) Howard, J. *Annu. Rev. Physiol.* **1996**, *58*, 703–29.
(12) Vale, R. D.; Funatsu, T.; Pierce, D. W.; Romberg, L.; Harada, Y.; Yanagida, T. *Nature* **1996**, *380* (6573), 451–453.
(13) Hiratsuka, Y.; Tada, T.; Oiwa, K.; Kanayama, T.; Uyeda, T. Q. *Biophys. J.* **2001**, *81* (3), 1555–1561.
(14) Moorjani, S. G.; Jia, L.; Jackson, T. N.; Hancock, W. O. *Nano Lett.* **2003**, *3* (5), 633–637.
(15) van den Heuvel, M. G. L.; Butcher, C. T.; Smeets, R. M. M.; Diez, S.; Dekker, C. *Nano Lett.* **2005**, *5* (6), 1117–1122.
(16) Lin, C. T.; Kao, M. T.; Kurabayashi, K.; Meyhofer, E. *Small* **2006**, *2* (2), 281–287.
(17) van den Heuvel, M. G. L.; Butcher, C. T.; Lemay, S. G.; Diez, S.; Dekker, C. *Nano Lett.* **2005**, *5* (2), 235–241.
(18) Kim, T.; Kao, M. T.; Hasselbrink, E. F.; Meyhofer, E. *Nano Lett.* **2007**, *7* (1), 211–217.
(19) Bachand, G. D.; Rivera, S. B.; Boal, A. K.; Gaudioso, J.; Liu, J.; Bunker, B. C. *Nano Lett.* **2004**, *4* (5), 817–821.
(20) Bachand, G. D.; Rivera, S. B.; Carroll-Portillo, A.; Hess, H.; Bachand, M. *Small* **2006**, *2* (3), 381–385.
(21) Ramachandran, S.; Ernst, K. H.; Bachand, G. D.; Vogel, V.; Hess, H. *Small* **2006**, *2* (3), 330–334.
(22) Boal, A. K.; Tellez, H.; Rivera, S. B.; Miller, N. E.; Bachand, G. D.; Bunker, B. C. *Small* **2006**, *2* (6), 793–803.
(23) Diez, S.; Reuther, C.; Dinu, C.; Seidel, R.; Mertig, M.; Pompe, W.; Howard, J. *Nano Lett.* **2003**, *3* (9), 1251–1254.
(24) Engvall, E.; Perlman, P. *Immunochemistry* **1971**, *8* (9), 871–874.
(25) Nam, J. M.; Thaxton, C. S.; Mirkin, C. A. *Science* **2003**, *301* (5641), 1884–1886.
(26) Zheng, G. F.; Patolsky, F.; Cui, Y.; Wang, W. U.; Lieber, C. M. *Nat. Biotechnol.* **2005**, *23* (10), 1294–1301.
(27) Wu, G. H.; Datar, R. H.; Hansen, K. M.; Thundat, T.; Cote, R. J.; Majumdar, A. *Nat. Biotechnol.* **2001**, *19* (9), 856–860.
(28) Gerdon, A. E.; Wright, D. W.; Cliffel, D. E. *Anal. Chem.* **2005**, *77* (1), 304–310.
(29) Chou, S. F.; Hsu, W. L.; Hwang, J. M.; Chen, C. Y. *Biosens. Bioelectron.* **2004**, *19* (9), 999–1005.

NL072742X